

Noninvasive multiphoton fluorescence microscopy resolves retinol and retinal condensation products in mouse eyes

Grazyna Palczewska¹, Tadao Maeda^{2,3}, Yoshikazu Imanishi³, Wenyu Sun¹, Yu Chen³, David R Williams⁴, David W Piston⁵, Akiko Maeda^{2,3} & Krzysztof Palczewski^{1,3}

© 2010 Nature America, Inc. All rights reserved.

Multiphoton excitation fluorescence microscopy (MPM) can image certain molecular processes *in vivo*. In the eye, fluorescent retinyl esters in subcellular structures called retinosomes mediate regeneration of the visual chromophore, 11-*cis*-retinal, by the visual cycle. But harmful fluorescent condensation products of retinoids also occur in the retina. We report that in wild-type mice, excitation with a wavelength of ~730 nm identified retinosomes in the retinal pigment epithelium, and excitation with a wavelength of ~910 nm revealed at least one additional retinal fluorophore. The latter fluorescence was absent in eyes of genetically modified mice lacking a functional visual cycle, but accentuated in eyes of older wild-type mice and mice with defective clearance of all-*trans*-retinal, an intermediate in the visual cycle. MPM, a noninvasive imaging modality that facilitates concurrent monitoring of retinosomes along with potentially harmful products in aging eyes, has the potential to detect early molecular changes due to age-related macular degeneration and other defects in retinoid metabolism.

High-resolution noninvasive imaging has become an essential method for understanding complex biological systems in experimental cell lines and is used with increasing frequency in tissues and live animals^{1–5}. These methods are also being slowly adapted for diagnostic testing and clinical applications, where they show great promise^{2,6,7}. Two-photon microscopy (TPM) offers real time, high-resolution images of endogenous fluorescent molecules in living tissues with little or no tissue damage^{8–11}. Use of long-wavelength and nonlinear excitation bypasses absorption by ultraviolet and visible light chromophores and allows imaging at low laser power with subcellular resolution at tissue depths not attainable with other noninvasive optical modalities. Vertebrate eyes have evolved to prevent short ultraviolet wavelength light from reaching the retina. Instead, infrared illumination used in MPM is ideal for visualizing fluorescent biomarkers that exist endogenously in retinal pigment epithelial (RPE) cells of the eye.

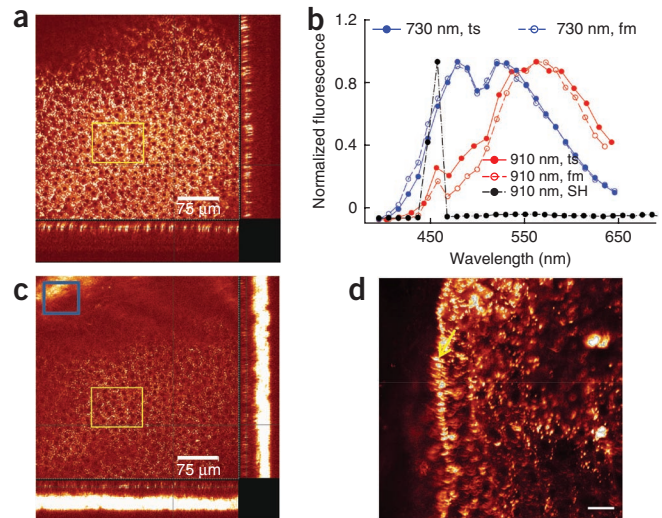
There are two types of fluorescent retinoids indicative of certain functional and disease states of human eyes. The intrinsic chromophore, fatty acid-esterified retinol, has weak fluorescence and has a propensity to cluster with phospholipids and helper proteins into structures called retinosomes located close to the RPE plasma membrane^{12–14}. Fatty acid-esterified retinol is generated by sequential reactions of the visual cycle (**Supplementary Fig. 1**). First, photoisomerization of 11-*cis*-retinylidene, the light-sensitive chromophore of visual pigments in rods and cones, generates all-*trans*-retinylidene, which is then hydrolyzed and reduced to retinol. Next, retinol is transported from photoreceptors to the RPE and esterified in a lecithin: retinol acyl transferase (LRAT)-dependent reaction; additionally, these esters are formed from retinol imported from the circulation¹⁵. As indicated by noninvasive *in vivo* TPM imaging through the sclera, and by chemical analyses of eyes of wild-type (WT) and genetically modified mice, retinosomes accumulate fatty acid-esterified retinol essential for 11-*cis*-retinal production. Thus, retinosomes serve as the reservoir of all-*trans*-retinyl esters for dynamic transfer and conversion of retinoids in the eye.

Condensation products of all-*trans*-retinal are also fluorescent, and their accumulation within the RPE is indicative of aging retina or retinal pathology. These stable condensation products, including A2E (2-[2,6-dimethyl-8-(2,6,6-trimethyl-1-cyclohexen-1-yl)-1E,3E,5E,7E-octatetraenyl]-1-(2-hydroxyethyl)-4-[4-methyl-6-(2,6,6-trimethyl-1-cyclohexen-1-yl)-1E,3E,5E-hexatrienyl]-pyridinium), A2DHP-PE (phosphatidyl-dihydropyridine bisretinoid) and all-*trans*-retinal dimers¹⁶ that result from inadequate clearance and conversion of all-*trans*-retinal back to 11-*cis*-retinol through the visual cycle^{17,18}, comprise the lipofuscin of RPE. All-*trans*-retinal itself is a reactive cytotoxic aldehyde that can damage the retina^{17,18}, but the relative toxicities of its condensation products have not been fully clarified. Several explanations for such toxicity have been proposed, including complement activation^{19,20}, destruction of membrane structures¹⁶ and photooxidative damage by acting as a chromophore for blue light²¹. Retinyl esters and all-*trans*-retinal condensation products must be spectrally resolved to monitor their status independently.

¹Polgenix, Cleveland, Ohio, USA. ²Department of Ophthalmology and Visual Sciences, Case Western Reserve University, Cleveland, Ohio, USA. ³Department of Pharmacology, Case Western Reserve University, Cleveland, Ohio, USA. ⁴Center for Visual Science, University of Rochester, Rochester, New York, USA. ⁵Department of Molecular Physiology and Biophysics, Vanderbilt University, Nashville, Tennessee, USA. Correspondence should be addressed to K.P. (kxp65@case.edu) or G.P. (gpalczewski@polgenixinc.com).

Received 27 April; accepted 3 August; published online 14 November 2010; doi:10.1038/nm.2260

Figure 1 Multiphoton excitation of a 6-month-old WT mouse eye at 730 and 910 nm produced emission spectra indicating more than one fluorophore. **(a)** A series of TPM images of an intact mouse eye were obtained along the axis perpendicular to the RPE layer with an excitation wavelength of 730 nm. The main box reveals the *en face* image of RPE cells; the two cross-section images, one shown at the bottom and the other at the right edge, were assembled from a series of Z-slice images. The yellow outlined rectangle represents the region from which fluorescence was collected for spectral analysis with the excitation light focused on the RPE. **(b)** Fluorescence emission spectra from the RPE of an intact mouse eye through the sclera (ts) and from flat-mounted (fm) mouse RPE. The second harmonic signal (SH) shows a sharp maximum at half of the 910-nm excitation wavelength. **(c)** A series of TPM images of an intact mouse eye obtained with an excitation wavelength of 910 nm. In the region of the blue outlined rectangle, a strong second harmonic signal from the sclera was dominant, as the curvature of the eye brought the sclera more into focus. The yellow outlined rectangle represents the region from which fluorescence was collected for spectral analysis shown in **b**. **(d)** TPM image of flat-mounted *ex vivo* RPE. Part of the RPE is folded over, exposing a sagittal view of retinosomes, indicated with the yellow arrow. Scale bar, 20 μ m.



Herein we describe studies that extend the use of noninvasive multiphoton fluorescence microscopy to the study of native tissues within the eye. Spectral analyses of fluorophores activated at two different wavelengths and chemical analyses of the eyes in mice with different genetic backgrounds revealed distinguishing features between retinosomes and condensation products of all-*trans*-retinal associated with retinal pathology. Imaging methods described herein could be highly useful to assess the outcome of pharmacological interventions.

RESULTS

Fluorescent images of the RPE excited by an infrared laser

Consistent with previously published results^{12–14}, we identified retinosomes in the RPE of mice by using a 730-nm femtosecond (fs) laser (**Fig. 1a**). The emission spectrum analyzed from fluorescence obtained from the area outlined by the yellow rectangle in **Figure 1a** showed two maxima at 480 nm and 521 nm (**Fig. 1b**). This spectrum was superimposable with that of authentic all-*trans*-retinol solution in ethanol obtained under identical experimental conditions (**Supplementary Fig. 2a**). The two-photon spectra differed from those derived from ultraviolet excitation

of retinol that produced a much stronger emission at 480 nm, as compared to the 521 nm peak, which only appeared as a shoulder. This difference probably resulted from a complex electron excitation-relaxation structure for this conjugated polyene, wherein the lower energy component is enhanced by two-photon excitation. Retinol also emits fluorescence at longer excitation wavelengths (**Supplementary Fig. 2a**), so we analyzed the RPE with an excitation wavelength of 910 nm (**Fig. 1c**). Although we observed a strong fluorescence, it differed from that of retinosomes by having a maximal emission at \sim 570 nm (**Fig. 1b**), suggesting the presence of fluorophores other than retinol within the RPE. We also observed a very strong second harmonic signal derived from the sclera (**Fig. 1b,c**) that probably originated from collagen-enriched structures⁹. Fluorescence emission spectra were the same whether images were obtained directly from flat-mounted RPE or through the sclera of the intact eye (**Fig. 1b,d**).

Images taken as a function of excitation wavelengths with constant laser power and detector setting revealed that the high-fluorescence emission observed at 720 nm excitation decreased until 850 nm and then increased again at 910 nm (**Fig. 2a**). However, the well-defined fluorescent pattern of retinosomes obtained with 730-nm excitation (**Fig. 2b**) was replaced with more uniformly distributed cellular structures at the longer 910-nm excitation wavelength (**Fig. 2c**). Moreover, the spectrum systematically shifted from a shorter- to a longer-wavelength emission as the excitation wavelength increased from 720 nm to 910 nm (**Supplementary Fig. 2b**).

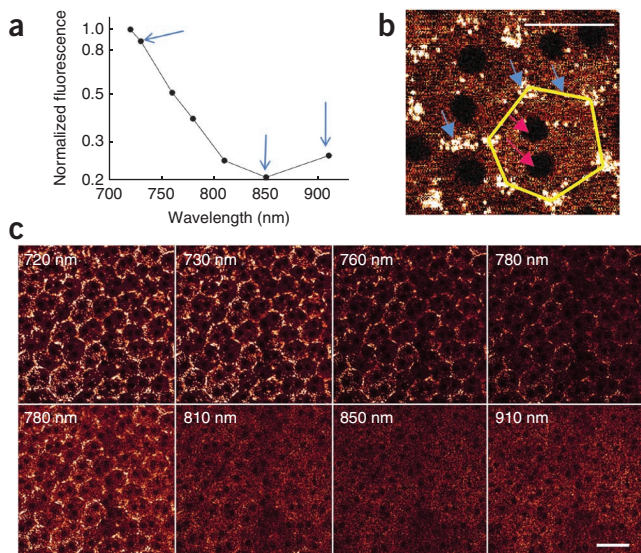


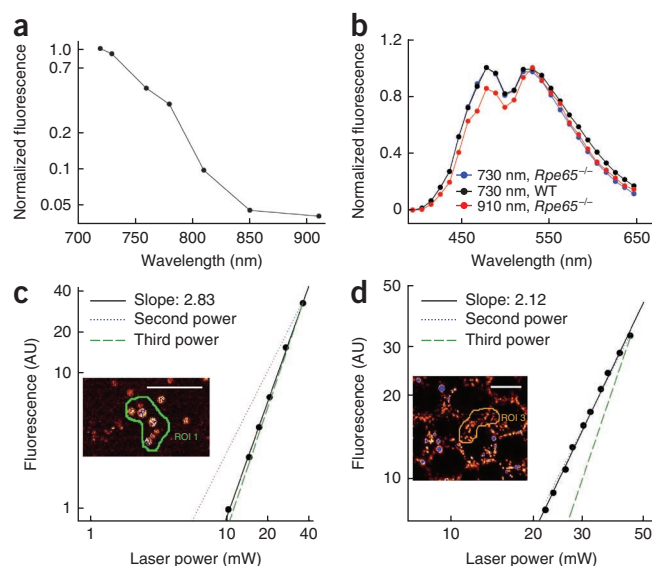
Figure 2 Multiphoton excitation of the RPE in an intact 6-month-old WT mouse eye at different wavelengths of excitation light. **(a)** Graph showing fluorescence as a function of excitation light wavelength. Fluorescence intensities were obtained as mean pixel values from the area covered by at least 20 RPE cells in focus and were normalized to the maximum value at 720 nm. Blue arrows (from left to right) indicate fluorescence in response to 730-, 850- and 910-nm excitation. **(b)** Zoomed-in two-photon image of RPE cells obtained with 730-nm excitation. Blue arrowheads denote retinosomes (white) clustering along plasma membranes; the edges of one RPE cell are highlighted in yellow. Dark, mostly double nuclei are indicated by pink arrowheads. Scale bar, 25 μ m. **(c)** Images of RPE cells at the excitation wavelengths indicated in each image. All images were obtained with 10 mW of laser power. Photomultiplier tube (PMT) gain and offset were kept constant for the images in the top row. Then the gain was readjusted and kept constant for the images in the bottom row. Scale bar, 38 μ m.

Figure 3 Visualization of retinosomes by three-photon excitation spectroscopy in the intact 7-week-old *Rpe65*^{-/-} mouse eye. (a) Graph showing fluorescence intensity as a function of excitation light wavelength; fluorescence intensity was calculated as a mean pixel value from the area covered by at least 20 RPE cells in focus during imaging and normalized to the maximum value at 720 nm excitation. (b) Emission spectra from the RPE of WT and *Rpe65*^{-/-} mouse eyes excited with laser light at 730 nm and 910 nm. (c) Logarithmic plot of fluorescence intensity as a function of excitation power shows evidence of three-photon excitation at an excitation wavelength of 910 nm. AU, arbitrary units. (d) Logarithmic plot of fluorescence intensity as a function of excitation power shows evidence of three-photon excitation at an excitation wavelength of 730 nm. In c and d, data points are shown as black circles. Modeling of the pure second-power dependence is shown by the blue dotted line and modeling of the third-power dependence is indicated by the green dashed line. Insets depict areas containing the retinosomes from which fluorescence was quantified. Scale bars, 20 μm.

Three-photon excitation of retinosomes

If the unidentified fluorophores emitting in response to 910 nm excitation were condensation products of all-*trans*-retinal produced from bleached visual pigments¹⁶, they should be absent in retinal pigment epithelium-specific 65-kDa protein (Rpe65)-knockout mice, which have a defective visual cycle²². Fluorescence as a function of increasing excitation light wavelength in these mice showed a monotonic decay with no increase in signal observed at 910 nm (Fig. 3a, Supplementary Fig. 3). Excitation at either 730 nm or 910 nm elicited the same emission spectrum (Fig. 3b), suggesting that retinyl esters are visible with both 730 nm and 910 nm excitation. Moreover, the emission spectrum was consistent with those derived from WT mice with 730-nm excitation (Fig. 3b). We further confirmed our identification of retinosomes in *Rpe65*^{-/-} mice by gavaging these mice with artificial chromophore^{23,24}. We observed expansion of retinosomes and increased retinyl ester content after we treated these mice with 9-*cis*-retinyl acetate (Supplementary Fig. 4).

All-*trans*-retinyl esters or retinol show a maximal emission at ~480 nm, with a shoulder at longer wavelengths when examined in a mixture of organic solvents (Supplementary Fig. 5a)²⁵. The fluorescence of retinosomes in retinas of *Rpe65*^{-/-} mice subjected to two-photon excitation with 910 nm should be negligible, given that the optical density of retinol (or retinyl esters) at half this wavelength, that



is, 455 nm, is only 0.3% of that at 365 nm (half of 730 nm) with single-photon excitation in hexane (Supplementary Fig. 5b). Moreover, the optical density at 303 nm for retinol should be 64% of its maximal absorption at 326 nm; thus, it is more likely that the 910 nm-induced signal is the result of three-photon excitation. Accordingly, we found that retinyl esters are indeed excited by simultaneous absorption of three 910-nm photons. The probability of excitation by three-photon excitation is proportional to light intensity cubed, whereas the probability by two-photon excitation is proportional to the light intensity squared. At an excitation wavelength of 910 nm, fluorescence emission was proportional to the 2.83rd power of the excitation intensity (Fig. 3c), indicating a substantial contribution of the three-photon effect. The third-power dependence, rather than the second-power dependence, showed good agreement with the data. At an excitation wavelength of 730 nm, fluorescence was proportional to the 2.12th power (Fig. 3d), consistent with a two-photon effect.

High levels of A2E in mice with defective retinoid cycle

Mice lacking retinoid cycle enzymes *Abca4* and *Rdh8* (Supplementary Fig. 1) show both deficient transport of all-*trans*-retinal from the internal discs and a reduced capacity for all-*trans*-retinal reduction and clearance^{18,26,27}. Consequently, *Abca4*^{-/-};*Rdh8*^{-/-} mice accumulate large amounts of A2E and other all-*trans*-retinal condensation products. Images obtained with wavelengths of excitation light that increased from 720 nm to 910 nm were consistently brighter than those from WT mice (Fig. 4a), with exceptionally high fluorescence at 910 nm. Spectra with 730-nm excitation showed the emission peak characteristic for either retinol or retinyl ester together with a peak at about 560 nm attributable to retinal condensation products (Fig. 4b). As expected, the contribution of retinosomes to

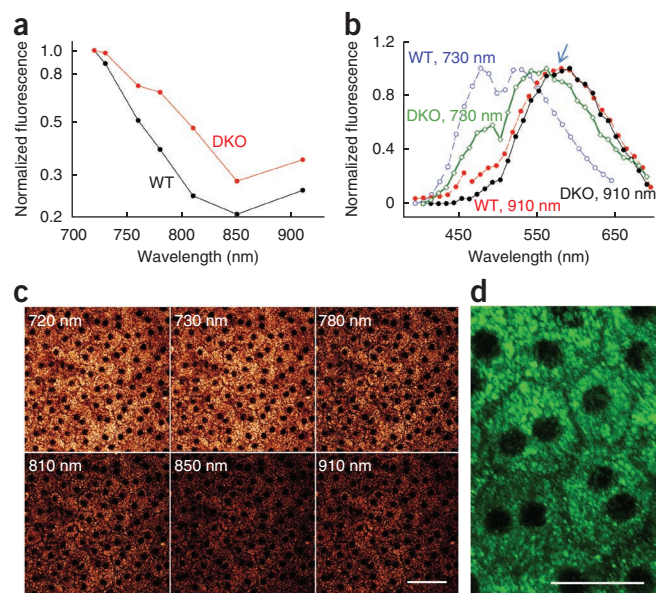


Figure 4 Two-photon excitation of 3-month-old *Abca4*^{-/-};*Rdh8*^{-/-} (DKO) intact mouse eye. (a) Fluorescence intensity as a function of excitation wavelength, normalized to maximum emission at 720 nm excitation. (b) Emission spectra from RPE of WT and DKO mice excited with laser light at 730 nm and 910 nm. Blue arrow points to 580 nm. (c) Images of DKO mouse RPE at the indicated excitation wavelengths. All images were obtained with 10 mW of laser power; photomultiplier tube gain and offset were kept constant. Scale bar, 50 μm. (d) Zoomed-in TPM image of unstained DKO mouse RPE. Green color was arbitrarily chosen to make the image details more visible. Scale bar, 25 μm.

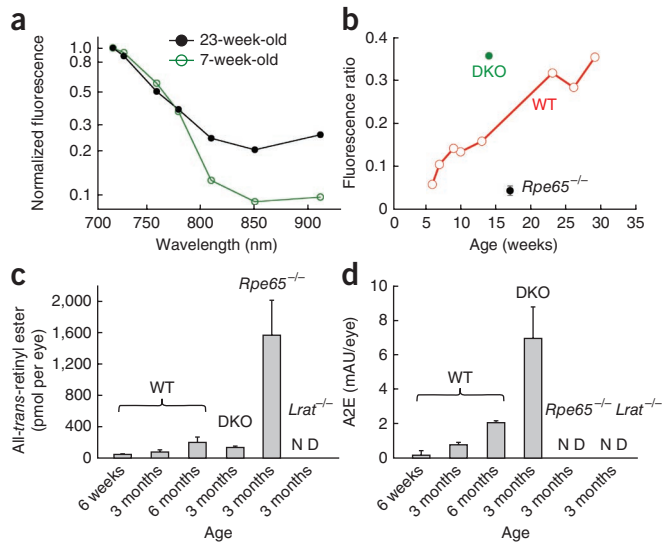


Figure 5 Age-dependent changes in fluorophore accumulation in mouse eyes. **(a)** The two-photon excitation fluorescence intensity as a function of wavelength in 23-week-old and 7-week-old WT mouse retina. Fluorescence emission values were normalized to that observed with 720-nm excitation. **(b)** Ratios of fluorescence excited with 910-nm light relative to fluorescence excited with 730-nm light. **(c)** Levels of all-*trans*-retinyl esters in the eyes of WT, DKO, *Rpe65*^{-/-} and *Lrat*^{-/-} mice of different ages ($n = 5$ for each group). **(d)** Levels of A2E extracted from WT, DKO, *Rpe65*^{-/-} and *Lrat*^{-/-} mouse eyes of different ages ($n = 5$ for each group). In **c** and **d**, data are means \pm s.d. ND, not detected.

this emission spectrum was reduced. Notably, the bright fluorescence, although punctate, was spread throughout cells (**Fig. 4c,d**) at all wavelengths tested (**Fig. 4c**). Synthetic A2E standard had a similar emission spectrum, with the maximum shifted to the longer wavelength when examined by two-photon excitation (**Supplementary Fig. 2a**), an observation similar to previous findings²⁸. These results and those obtained with WT, *Lrat*^{-/-} and *Rpe65*^{-/-} mice (**Supplementary Fig. 6**) strongly correlate with levels of all-*trans*-retinyl esters and A2E found in the retinas of these mice (**Fig. 5**). Because A2E accumulates with age, images obtained with excitation wavelengths of 730 nm and 910 nm could be extremely helpful in discriminating between essential retinoids of the visual cycle, such as retinols and retinyl esters present in retinosomes, and potentially harmful retinoids, such as excessive amounts of all-*trans*-retinal and its condensation products.

Two-photon imaging to detect retinal aging

To test the ability of TPM to detect retinal aging, we obtained fluorescence images from WT mice at various ages and with multiple excitation wavelengths (**Fig. 5a**). Fluorescence emission decreased markedly with increasing excitation wavelengths in 7-week-old mice, but in 23-week-old mice fluorescence emission at longer wavelengths was elevated (**Fig. 5a**). Therefore, we systematically evaluated ratios of fluorescence obtained with 910 nm excitation to the fluorescence with 730 nm excitation and plotted these ratios as a function of age (**Fig. 5b**). As expected, WT mice showed an increase in these ratios as a function of age, presumably because A2E and other all-*trans*-retinal condensation products accumulated. Moreover, 14-week-old control *Abca4*^{-/-}; *Rdh8*^{-/-} mice with significantly elevated A2E had a very high 910 nm / 730 nm fluorescence ratio, whereas 17-week-old *Rpe65*^{-/-} mice, which do not produce A2E, had a very low ratio²², even below that of young WT mice. We then tested the level of retinyl

esters as a function of age and found that this retinoid accumulates with age, as previously observed (**Fig. 5c**)²⁴. Of note, A2E abundance increased with age, as well (**Fig. 5d**). In the presence of both A2E and all-*trans*-retinyl esters in WT and *Abca4*^{-/-}; *Rdh8*^{-/-} mice, we observed much more fluorescence from A2E, because excitation of A2E seems to be more efficient at the longer wavelengths than the three-photon excitation of retinyl esters. This was indicated by increased levels of fluorescence at longer wavelengths. At longer excitation wavelengths, the two-photon emission spectrum of lipofuscin in human RPE overlaps the spectrum of WT mouse RPE (**Supplementary Fig. 7**).

DISCUSSION

The aims of this study were to optimize multiphoton imaging of retinosomes, use multiphoton spectroscopy to distinguish among retinal fluorophores and examine the use of noninvasive multiphoton spectroscopy to monitor changes in the retina caused by inherited visual disorders and aging.

Our study reveals that autofluorescent images of the retina, specifically of the RPE, can be obtained at two excitation wavelengths, one at \sim 730 nm and the other at \sim 910 nm. Excitation with \sim 730-nm photons clearly images retinosomes in the two-photon mode, whereas \sim 910-nm photons primarily excite fluorophores related to the condensation of all-*trans*-retinal, for example, A2E, A2DHP-PE and retinal dimers¹⁶. Only under special circumstances can retinosomes be imaged with \sim 910-nm photons, as in *Rpe65*^{-/-} mice, where they are enlarged. In such cases, nearly simultaneous absorption of two and even three photons can take place. These findings are consistent with the maximal absorption of all-*trans*-retinyl esters or all-*trans*-retinol at 326 nm (**Supplementary Fig. 5**) and A2E at \sim 440 nm¹⁶. There are several differences between retinosomes and retinoid-condensation products. Retinosomes are located close to the plasma membrane and are surrounded by adipose differentiation-related protein¹², whereas condensation products are spread throughout the cell. Each has a fluorescence emission spectrum unique to its chemical and cellular structures, and all-*trans*-retinal condensation products not only accumulate with age but also are either highly elevated or absent in mice with deletions of certain genes encoding enzymes of the visual cycle. Condensation products are proposed to be generated in photoreceptors and accumulated in lysosomes of the RPE, and the distribution of condensation products observed here (**Figs. 2 and 4**) fits this description¹³.

In the RPE, levels of all-*trans*-retinal condensation products increase with age¹⁶, because each day about 10% of a human's rod outer segments, where these products are formed, are shed and phagocytosed by RPE cells²⁹. These conjugates accumulate within the RPE because their breakdown is either slow or nonexistent in mammals. Even though we clearly observed fluorescent retinosomes in mice when fluorescence was measured upon excitation at 730 nm and 910 nm, emission from condensation products was dominant upon 910-nm excitation. Thus, it seems that the emission fluorescence ratio after excitation at these two wavelengths, that is, the 910 nm / 730 nm ratio, might be used to monitor the health of the retina and evaluate the efficacy of therapeutic agents, at least in mice.

The total background autofluorescence of the fundus examined by scanning laser ophthalmoscopy (SLO) at the same laser power (sensitivity at 100) also reflected the amounts of A2E in mice (**Supplementary Fig. 8** and **Fig. 5d**). However, because adjustments in laser power are required for each individual to compensate for various eye conditions such as cataracts, direct comparison

of SLO values between individuals and time points poses potential problems. Moreover, the infrared laser of current SLO cannot cause two-photon excitation. Therefore, the 910 nm / 730 nm excitation ratio of TPM offers a greater advantage in assessing the health of the retina.

TPM provides several advantages over single-photon microscopy in monitoring the human eye. The human lens and macular pigments are highly opaque to ultraviolet and blue light, respectively. Therefore, it is especially difficult to deliver excitation light safely and efficiently to ultraviolet- and blue-absorbing fluorophores in the macula. Instead of using short-wavelength excitation, TPM takes advantage of infrared illumination to excite ultraviolet- and blue-absorbing fluorophores such as retinyl esters and A2E, whose dynamics and quantities change in the macula of people with pre-age-related macular degeneration (AMD). In AMD, increasing RPE fluorescence is one of the earliest changes observed³⁰. A recent large-scale prospective study of individuals with geographic atrophy showed that fundus autofluorescence at the margins of geographic atrophy was the best predictor of geographic atrophy progression. The unique ability of TPM to simultaneously image intermediates and byproducts of the visual cycle in the intact eye enables monitoring formation of all-*trans*-retinal condensation products *in vivo* by comparing the ratio of fluorescence excited with 730 nm to 910 nm. Moreover, as observed by us and others, the all-*trans*-retinal levels required to produce toxicity *in vitro* (5 μM) are also found *in vivo*, especially after bright light exposure. A lifetime of light exposure has been proposed as one of several risk factors for advanced AMD^{18,31}.

Other advantages of TPM include less light scattering with resultant deeper penetration, intrinsic three-dimensionality and a decreased risk of photobleaching and phototoxicity. TPM is also a growing technology with potential applications to both basic science and clinical research³². However, most current TPM applications use exogenous fluorescent markers rather than endogenous fluorophores, and most other procedures involving larger organisms are invasive.

By taking advantage of an animal model for Leber congenital amaurosis (the *Rpe65*^{-/-} mouse) we quantitatively determined that three-photon microscopy can generate a fluorescent image characteristic of this disease. Three-photon microscopy requires three photons to be absorbed per fluorescent event, and the excitation is proportional to the instantaneous intensity of incident laser light (*I*) to the third power. If imaging conditions are identical, the ratio of three-photon-excited fluorescence to two-photon-excited fluorescence is proportional to $\delta_3 \times I / \delta_2$, where δ_2 is the two-photon excitation cross-section and δ_3 is the three-photon excitation cross-section¹¹. We are not aware of any data directly dealing with two or three-photon excitation cross sections as a function of wavelength for all-*trans*-retinyl esters, so we used existing data for retinol instead³³. On the basis of several assumptions, we calculated whether three-photon excitation of retinyl esters might occur at 910 nm. We assumed that the two- and three-photon fluorescence quantum yields (η) are the same, that the three-photon excitation cross-section spectrum is offset from the two-photon excitation cross-section spectrum by a factor of 10^{-33} (ref. 11), and that it parallels the two-photon excitation spectrum if the wavelengths are set to 1.5 -times the corresponding two-photon process wavelengths. Then, using data for the wavelength-dependent two-photon fluorescence action cross section of retinol ($\eta \times \delta_2$), we estimate that at 910 nm, $\eta \times \delta_2 \approx 8.8 \times 10^{-56}$ cm⁴ s per photon, and, taking into account that maximum absorption of retinol is at 326 nm (Supplementary Fig. 5), we estimate that

three-photon cross section extrapolates to $\eta \times \delta_3 \approx 1.8 \times 10^{-86}$ cm⁶ s² per photon². Using these numbers and the intensity at 910 nm,

$$I_{910} \approx (p_o \times \pi \times (NA)^2) / (f_p \times \tau_p \times h \times c \times \lambda) = 1.5 \times 10^{30} \text{ photons per cm}^2 \text{ s}$$

where *c* is the speed of light, *h* is Planck's constant, *NA* is the numerical aperture, *p_o* is the average incident power, τ_p is the pulse duration, *f_p* is the pulse repetition frequency and λ is the pulse center wavelength³⁴, we calculate that at 910 nm the ratio $\delta_3 \times I / \delta_2 \approx 0.3$. Following the same methodology but now at 730 nm, we calculated $I_{730} \approx 1.9 \times 10^{30}$ photons per cm² s, $\eta \times \delta_2 \approx 3 \times 10^{-52}$ cm⁴ s per photon, $\eta \times \delta_3 \approx 9.2 \times 10^{-89}$ cm⁶ s² per photon² and $\delta_3 \times I / \delta_2 \approx 6 \times 10^{-7}$. These estimates suggest that three-photon excitation of retinyl ester is feasible at 910 nm but not at 730 nm, supporting our experimental demonstration. Thus the three-photon effect has been demonstrated, perhaps for the first time, in the intact, unfixed fresh eye.

In summary, TPM of endogenous fluorophores, including retinyl esters, all-*trans*-retinol, and A2E, provides a powerful way to monitor the visual cycle¹⁵ directly and contribute to understanding the pathology of human retinal diseases. If we could visualize and understand early aberrations of these pathways in live human eyes, we would be better able to devise and monitor effective therapies for blinding retinal diseases.

METHODS

Methods and any associated references are available in the online version of the paper at <http://www.nature.com/naturemedicine/>.

Note: Supplementary information is available on the Nature Medicine website.

ACKNOWLEDGMENTS

We would like to thank M. Golczak for help during the course of this study and Z. Dong for expert handling of mice. We also thank L.T. Webster and members of Palczewski laboratory for critical comments on the manuscript. *Rpe65*^{-/-} mice were a kind gift from M. Redmond (US National Eye Institute). This research was supported in part by grants EY008061, EY009339, EY019880, EY019031, EY020715 and P30 EY11373 from the US National Institutes of Health, TECH 09-004 from the State of Ohio Department of Development and Third Frontier Commission, the European Life Scientist Organization and the Klaus Tschira Foundation.

AUTHOR CONTRIBUTIONS

G.P. and K.P. conceived of and directed the project. G.P., T.M., Y.I., W.S., Y.C. and A.M. designed and conducted experiments. G.P. and K.P. prepared the manuscript. Y.I., D.W.P. analyzed the data and edited the manuscript. D.R.W. edited the manuscript.

COMPETING FINANCIAL INTERESTS

The authors declare competing financial interests: details accompany the full-text HTML version of the paper at <http://www.nature.com/naturemedicine/>.

Published online at <http://www.nature.com/naturemedicine/>.

Reprints and permissions information is available online at <http://npg.nature.com/reprintsandpermissions/>.

- Schenke-Layland, K., Riemann, I., Damour, O., Stock, U.A. & Konig, K. Two-photon microscopes and *in vivo* multiphoton tomographs—powerful diagnostic tools for tissue engineering and drug delivery. *Adv. Drug Deliv. Rev.* **58**, 878–896 (2006).
- Zhang, E.Z., Laufer, J.G., Pedley, R.B. & Beard, P.C. *In vivo* high-resolution 3D photoacoustic imaging of superficial vascular anatomy. *Phys. Med. Biol.* **54**, 1035–1046 (2009).
- Kim, J.S. *et al.* Imaging of transient structures using nanosecond *in situ* TEM. *Science* **321**, 1472–1475 (2008).
- Shoham, D. *et al.* Imaging cortical dynamics at high spatial and temporal resolution with novel blue voltage-sensitive dyes. *Neuron* **24**, 791–802 (1999).
- Hell, S.W. Far-field optical nanoscopy. *Science* **316**, 1153–1158 (2007).
- DaCosta, R.S., Wilson, B.C. & Marcon, N.E. Optical techniques for the endoscopic detection of dysplastic colonic lesions. *Curr. Opin. Gastroenterol.* **21**, 70–79 (2005).

7. Evgenov, N.V., Medarova, Z., Dai, G., Bonner-Weir, S. & Moore, A. *In vivo* imaging of islet transplantation. *Nat. Med.* **12**, 144–148 (2006).
8. Piston, D.W. Imaging living cells and tissues by two-photon excitation microscopy. *Trends Cell Biol.* **9**, 66–69 (1999).
9. Imanishi, Y., Lodowski, K.H. & Koutalos, Y. Two-photon microscopy: shedding light on the chemistry of vision. *Biochemistry* **46**, 9674–9684 (2007).
10. Denk, W., Strickler, J.H. & Webb, W.W. Two-photon laser scanning fluorescence microscopy. *Science* **248**, 73–76 (1990).
11. Xu, C., Zipfel, W., Shear, J.B., Williams, R.M. & Webb, W.W. Multiphoton fluorescence excitation: new spectral windows for biological nonlinear microscopy. *Proc. Natl. Acad. Sci. USA* **93**, 10763–10768 (1996).
12. Imanishi, Y., Sun, W., Maeda, T., Maeda, A. & Palczewski, K. Retinyl ester homeostasis in the adipose differentiation-related protein-deficient retina. *J. Biol. Chem.* **283**, 25091–25102 (2008).
13. Imanishi, Y., Batten, M.L., Piston, D.W., Baehr, W. & Palczewski, K. Noninvasive two-photon imaging reveals retinyl ester storage structures in the eye. *J. Cell Biol.* **164**, 373–383 (2004).
14. Imanishi, Y., Gerke, V. & Palczewski, K. Retinosomes: new insights into intracellular managing of hydrophobic substances in lipid bodies. *J. Cell Biol.* **166**, 447–453 (2004).
15. von Lintig, J., Kiser, P.D., Golczak, M. & Palczewski, K. The biochemical and structural basis for *trans-to-cis* isomerization of retinoids in the chemistry of vision. *Trends Biochem. Sci.* **35**, 400–410 (2010).
16. Sparrow, J.R., Wu, Y., Kim, C.Y. & Zhou, J. Phospholipid meets all-trans-retinal: the making of RPE bisretinoids. *J. Lipid Res.* **51**, 247–261 (2010).
17. Maeda, A., Maeda, T., Golczak, M. & Palczewski, K. Retinopathy in mice induced by disrupted all-trans-retinal clearance. *J. Biol. Chem.* **283**, 26684–26693 (2008).
18. Maeda, A. *et al.* Involvement of all-trans-retinal in acute light-induced retinopathy of mice. *J. Biol. Chem.* **284**, 15173–15183 (2009).
19. Zhou, J., Jang, Y.P., Kim, S.R. & Sparrow, J.R. Complement activation by photooxidation products of A2E, a lipofuscin constituent of the retinal pigment epithelium. *Proc. Natl. Acad. Sci. USA* **103**, 16182–16187 (2006).
20. Zhou, J., Kim, S.R., Westlund, B.S. & Sparrow, J.R. Complement activation by bisretinoid constituents of RPE lipofuscin. *Invest. Ophthalmol. Vis. Sci.* **50**, 1392–1399 (2009).
21. Sparrow, J.R. *et al.* Involvement of oxidative mechanisms in blue-light-induced damage to A2E-laden RPE. *Invest. Ophthalmol. Vis. Sci.* **43**, 1222–1227 (2002).
22. Katz, M.L. & Redmond, T.M. Effect of Rpe65 knockout on accumulation of lipofuscin fluorophores in the retinal pigment epithelium. *Invest. Ophthalmol. Vis. Sci.* **42**, 3023–3030 (2001).
23. Van Hooser, J.P. *et al.* Rapid restoration of visual pigment and function with oral retinoid in a mouse model of childhood blindness. *Proc. Natl. Acad. Sci. USA* **97**, 8623–8628 (2000).
24. Van Hooser, J.P. *et al.* Recovery of visual functions in a mouse model of Leber congenital amaurosis. *J. Biol. Chem.* **277**, 19173–19182 (2002).
25. Drabent, R., Bryl, K. & Olszewska, T. A water environment forces retinyl palmitate to create self-organized structures in binary solvents. *J. Fluoresc.* **7**, 347–355 (1997).
26. Maeda, A., Golczak, M., Maeda, T. & Palczewski, K. Limited roles of Rdh8, Rdh12, and Abca4 in all-trans-retinal clearance in mouse retina. *Invest. Ophthalmol. Vis. Sci.* **50**, 5435–5443 (2009).
27. Maeda, T., Maeda, A., Leahy, P., Saperstein, D.A. & Palczewski, K. Effects of long-term administration of 9-cis-retinyl acetate on visual function in mice. *Invest. Ophthalmol. Vis. Sci.* **50**, 322–333 (2009).
28. Sparrow, J.R., Parish, C.A., Hashimoto, M. & Nakanishi, K. A2E, a lipofuscin fluorophore, in human retinal pigmented epithelial cells in culture. *Invest. Ophthalmol. Vis. Sci.* **40**, 2988–2995 (1999).
29. Kevany, B.M. & Palczewski, K. Phagocytosis of retinal rod and cone photoreceptors. *Physiology (Bethesda)* **25**, 8–15 (2010).
30. Holz, F.G. *et al.* Progression of geographic atrophy and impact of fundus autofluorescence patterns in age-related macular degeneration. *Am. J. Ophthalmol.* **143**, 463–472 (2007).
31. Wielgus, A.R., Chignell, C.F., Ceger, P. & Roberts, J.E. Comparison of A2E cytotoxicity and phototoxicity with all-trans-retinal in human retinal pigment epithelial cells. *Photochem. Photobiol.* **86**, 781–791 (2010).
32. So, P.T., Dong, C.Y., Masters, B.R. & Berland, K.M. Two-photon excitation fluorescence microscopy. *Annu. Rev. Biomed. Eng.* **2**, 399–429 (2000).
33. Zipfel, W.R. *et al.* Live tissue intrinsic emission microscopy using multiphoton-excited native fluorescence and second harmonic generation. *Proc. Natl. Acad. Sci. USA* **100**, 7075–7080 (2003).
34. Xu, C. & Webb, W.W. Measurement of two-photon excitation cross sections of molecular fluorophores with data from 690 to 1050 nm. *J. Opt. Soc. Am. B* **13**, 481–491 (1996).
35. Maeda, A. *et al.* Role of photoreceptor-specific retinol dehydrogenase in the retinoid cycle *in vivo*. *J. Biol. Chem.* **280**, 18822–18832 (2005).
36. Batten, M.L. *et al.* Lecithin-retinol acyltransferase is essential for accumulation of all-trans-retinyl esters in the eye and in the liver. *J. Biol. Chem.* **279**, 10422–10432 (2004).
37. Redmond, T.M. *et al.* Rpe65 is necessary for production of 11-cis-vitamin A in the retinal visual cycle. *Nat. Genet.* **20**, 344–351 (1998).
38. Batten, M.L. *et al.* Pharmacological and rAAV gene therapy rescue of visual functions in a blind mouse model of Leber congenital amaurosis. *PLoS Med.* **2**, e333 (2005).
39. Imanishi, Y. & Palczewski, K. Visualization of retinoid storage and trafficking by two-photon microscopy. *Methods Mol. Biol.* **652**, 247–261 (2010).
40. Maiti, S., Shear, J.B., Williams, R.M., Zipfel, W.R. & Webb, W.W. Measuring serotonin distribution in live cells with three-photon excitation. *Science* **275**, 530–532 (1997).

ONLINE METHODS

Mice. *Lrat*^{-/-} and *Rpe65*^{-/-} mice on a C57BL/6J background were crossed with C57 albino WT C57BL/6J-*Tyr*^{C-2J} mice to produce albino *Lrat*^{-/-} and *Rpe65*^{-/-} mice. *Rpe65*^{-/-} mice were a kind gift from M. Redmond; *Lrat*^{-/-} mice were generated in house³⁶. C57BL/6J mice were purchased from Harlan. Albino *Abca4*^{-/-}; *Rdh8*^{-/-} double-knockout mice were generated by crossing *Abca4*^{-/-}; *Rdh8*^{-/-} mice with a mixed 129Sv and C57BL/6J background^{17,35} with 129/SvJ albino WT mice (Jackson Laboratory). PCR genotyping of these mice was performed as previously described^{17,35-37}. Mice were housed and crossbred in the Case Western Reserve University Animal Resource Center Facility, where they were maintained under either a 12-h light-dark illumination cycle or in complete darkness. Manipulations in the dark were performed under dim red light transmitted through a filter (transmittance 560 nm; No. 1 Safelight; Eastman Kodak). Mice were provided free access to a standard chow diet and water. Prior to experimental analyses, they were anesthetized by intraperitoneal injection with 10 μ l per g body weight of 6 mg ml⁻¹ ketamine and 0.44 mg ml⁻¹ xylazine and then killed by cervical dislocation. All mouse procedures were approved by the Case Western Reserve University Animal Resource Center Facility Animal Care and Use Committee and complied with the American Veterinary Medical Association Guidelines on Euthanasia. Mice were gavaged with 9-*cis*-retinyl acetate according to a previously published protocol³⁸.

Retinoid and A2E Analyses. All experimental procedures related to extraction, derivatization and separation of retinoids from dissected mouse eyes were carried out as previously described^{17,35}. A2E was synthesized from all-*trans*-retinal and ethanolamine and purified by HPLC³⁵. Quantification of A2E after HPLC was accomplished by comparison with known concentrations of pure synthetic A2E standards³⁵.

Multiphoton excitation microscopy. TPM imaging was done with a Leica TCS SP2. A Ti:Sapphire laser (Coherent Chameleon XR) delivered <140-fs laser pulses at 90 MHz. The excitation light was focused on samples by a Planapochromat 1.25-numerical aperture, 0.1-mm working distance objective lens, and fluorescence was collected through the same lens. Fluorescence intensities and cross-section images were obtained by offline analyses with Leica LCS Lite software, version 4.0³⁹.

For imaging, a Hamamatsu R6357 photomultiplier tube was used as a non-descanned detector after filtering light through a band-pass Chroma filter, HQ 465/160. Before trans-scleral imaging and immediately after enucleation,

a mouse eye was placed at the center of a glass-bottomed 35-mm dish (MatTek), with the sclera contacting a coverslip and hydrated with solution of 9.5 mM sodium phosphate, pH 7.4, containing 137 mM NaCl and 2.7 mM KCl. The typical time between enucleation and data acquisition was less than 30 min. For flat-mount imaging, the cornea and lens were first dissected out of enucleated eyes with spring-loaded scissors, and the vitreous and retina were removed with tweezers. After four radial incisions, the RPE with choroid and sclera attached was laid in the center of a glass bottomed MaTek dish and directly imaged with its apical side facing the glass.

Emission spectra were obtained with a Leica TCS SP2 spectrally sensitive detector in the descanned configuration. Regions of interest were outlined with Leica LCS Lite software version 4.0. Spectra were normalized to the maximum value for each sample. The z-position on the microscope was kept constant when imaging with variable wavelength excitation, taking into account that retinosome size is greater than 4 μ m in the z direction, as deduced from **Figure 1**.

Characterization of fluorescence as a function of laser power. Imaging was done with 730-nm and 910-nm excitation wavelengths with 512 \times 512 pixels per frame and 400-Hz line speed. Pixel size was 0.367 μ m. Laser power was adjusted with a Leica TCS SP2 electro-optic modulator. At least 1 h was allowed for the laser to stabilize and electro-optic modulator to equilibrate with heat introduced by the infrared laser. Power was measured immediately before and after imaging in the sample plane with a calibrated Coherent FieldMax-TO laser power meter and a PM10 sensor. Laser power was measured by using the point bleach option with disabled scanning and blanking. To ensure that the laser beam was fully captured by the sensor, measurements used a FL PLAN 0.25-numerical aperture objective with a 17.6-mm working distance. To determine whether a two- or three-photon process was dominant, we first assumed that the two-photon excited fluorescence ($N_{\text{ex}2}$) was proportional to the incident laser power (p_0^2) and the two-photon fluorescence excitation cross section (δ_2)¹⁰, $N_{\text{ex}2} \approx \delta_2 \times p_0^2$; and that the three-photon-excited fluorescence was proportional to the p_0^3 and the three-photon fluorescence excitation cross section (δ_3)⁴⁰, $N_{\text{ex}3} \approx \delta_3 \times p_0^3$. Then the order of the process was determined from the slope of the line on the log-log plot.

Statistical analyses. Data are expressed as the means \pm s.d. Linear regression analysis of fluorescence as a function of laser power was performed with Sigma Plot. The square correlation (R^2) was calculated as higher than 0.997 for each case.